Osteoporosis International (2019) 30:1873–1885
https://doi.org/10.1007/s00198-019-05071-x

ORIGINAL ARTICLE

WNT3A accelerates delayed alveolar bone repair in ovariectomized mice

Y. Liu[1,2] · Z. Li[2,3] · M. Arioka[2,4] · L. Wang[1] · C. Bao[1] · J.A. Helms[2]

Received: 25 February 2019 / Accepted: 24 June 2019 / Published online: 23 July 2019

Abstract

Summary Our goal was to evaluate alveolar bone healing in OVX mice, and to assess the functional utility of a WNT-based treatment to accelerate healing in mice with an osteoporotic-like bony phenotype.

Introduction Is osteoporosis a risk factor for dental procedures? This relatively simple question is exceedingly difficult to answer in a clinical setting, for two reasons. First, as an age-related disease, osteoporosis is frequently accompanied by age-related co-morbidities that can contribute to slower tissue repair. Second, the intervals at which alveolar bone repair are assessed in a clinical study are often measured in months to years. This study aimed to evaluate alveolar bone repair in ovariectomized (OVX) mice and provide preclinical evidence to support a WNT-based treatment to accelerate alveolar bone formation.

Methods OVX was performed in young mice to produce an osteoporotic-like bone phenotype. Thereafter, the rate of extraction socket healing and osteotomy repair was assessed. A liposomal WNT3A treatment was tested for its ability to promote alveolar bone formation in this OVX-induced model of bone loss.

Results Bone loss was observed throughout the murine skeleton, including the maxilla, and mirrored the pattern of bone loss observed in aged mice. Injuries to the alveolar bone, including tooth extraction and osteotomy site preparation, both healed significantly slower than the same injuries produced in young controls. Given sufficient time, however, all injuries eventually healed. In OVX mice, osteotomies healed significantly faster if they were treated with L-WNT3A.

Conclusions Alveolar bone injuries heal slower in OVX mice that exhibit an osteoporotic-like phenotype. The rate of alveolar bone repair in OVX mice can be significantly promoted with local delivery of L-WNT3A.

Keywords Alveolar bone · Osteoporosis · Ovariectomy · Regeneration · WNT3A

Introduction

The clinical literature demonstrates that osteoporotic bones are more prone to fracture [1]. The basis for this increased risk lies in the mechanical function of the skeleton, which is derived from its structure [2]. In osteoporosis, the thickness, number, and connectivity of the bone trabeculae are reduced and coupled with thinning of the cortical bone [3]; these factors increase fracture risk for the osteoporotic skeleton [4]. In contrast, much less is known about whether osteoporosis affects fracture healing rates. This has led one expert to opine, "very little basic science or clinical research has been conducted that documents the effects of … osteoporosis on the healing of …fractures" [5].

In the intervening decade since that review, this knowledge gap has been addressed. Using animal models that mimic osteoporosis, the preclinical literature has clearly documented slower healing [6, 7]. The clinical literature also documents slower healing in osteoporotic patients [8]. These data, however, are oftentimes countered by websites claiming that "osteoporosis

Y. Liu, Z. Li and M. Arioka contributed equally to this work.

✉ J.A. Helms
jhelms@stanford.edu

[1] State Key Laboratory of Oral Diseases, National Clinical Research Center for Oral Diseases, West China Hospital of Stomatology, Sichuan University, 14 Third Section, Renmin Nan Road, Chengdu 610041, China

[2] Division of Plastic and Reconstructive Surgery, Department of Surgery, Stanford University School of Medicine, 1651 Page Mill Road, Palo Alto, CA 94304, USA

[3] Department of Orthopedics, Tianjin Medical University General Hospital, Tianjin 300052, China

[4] Department of Clinical Pharmacology, Faculty of Medical Sciences, Kyushu University, Fukuoka 812-8582, Japan

doesn't affect the healing process of bone. So if you do break a bone, rest assured it can heal as normal." [9].

When it comes to clarifying whether or not osteoporosis impacts fracture healing, the interrelationship between aging and the disease state becomes an obfuscating factor. Even healthy aging is associated with a deterioration in healing rates [10] in part because of chronic inflammation [11] and a decline in stem cell function (see [12] and reviewed in [13]). Due to these interconnected events, animal models have risen to the forefront as a means to study the disease state of osteoporosis. Here, we addressed how experimentally induced osteoporotic-like condition impacts the rate of bone healing, with a focus on alveolar bone of the jaws.

Like the appendicular and axial skeletons, the craniofacial skeleton is also affected by osteoporosis [14, 15], but unlike long bones and vertebrae, the effects are not readily apparent on X-rays [16]. Consequently, dental professionals oftentimes fail to appreciate the impact this systemic bone loss disease may have on their procedures such as implant osseointegration [17]. This ambiguity also presents a challenge in case planning because the majority of patients who receive dental implants are > 50 years of age [18] and thus are more likely to have osteoporosis or osteopenia [19].

We began this study with a relatively simple question: is osteoporosis a risk factor for dental procedures? We used a preclinical animal model that displays bony changes that are reminiscent of those seen in osteoporotic patients, and then carried out two surgical procedures that are equivalent to those performed in dental patients. In order to separate the multitudinous effects of aging from potential effects of osteoporosis, we produced an osteoporotic-like phenotype in an otherwise healthy young animal via ovariectomy (OVX) [20]. We established that the OVX surgery resulted in bony changes in the appendicular, axial, and most importantly for our study, alveolar bone. These OVX-induced changes resembled, from a structural perspective, what we also observed in an aged murine skeleton. We were then in a position to ask whether, in an otherwise young mouse, the OVX-induced osteoporotic-like state has a quantifiable effect on bone healing rates in the maxillae.

Materials and methods

Animals

The Stanford Committee on Animal Research approved all procedures, which conform to ARRIVE guidelines. In total, 66 mice were used, which included wild-type BALB/C females (Charles River Laboratories, Wilmington, MA) and $Axin2^{LacZ/+}$ females. $Axin2^{LacZ/+}$ mice have a BALB/C genetic background and are indistinguishable from non-genetically modified BALB/C mice [21]. In $Axin2^{LacZ/+}$ mice, one LacZ gene replaces the *Axin2* allele, resulting in translation of LacZ in Wnt-responsive cells [22]. Axin2 is a direct target of Wnt signaling [22]; therefore, the expression of the LacZ gene product, β-galactosidase, is a bona fide readout of Wnt pathway activity. To detect β-galactosidase activity, tissues were stained overnight at 37 °C in a solution containing 5 mM potassium ferricyanide, 5 mM potassium ferrocyanide, 2 mM $MgCl_2$, and 1 mg/ml X-gal (#B1690, Thermo Fisher Scientific).

Experimental groups

In keeping with the 3R's, every effort was made to reduce animal number [23]. Wherever possible and reasonable, the young control group of mice was shared between experiments. This sometimes led to small discrepancies between the ages of the test and control groups, but these differences were ~ 4% of the age of the animal [24]. Tables 1, 2, 3, 4, and 5 describe experimental groups, ages, genotypes, bone(s) being examined, and surgical/biochemical interventions, arranged to correspond with each figure.

Surgeries

Anesthesia was achieved via intraperitoneal ketamine/xylazine, while analgesia was ensured via subcutaneous Buprenorphine-SR (SR Veterinary Technologies, Fort Collins, CO). Dosages were calculated based on body weight.

Bilateral OVX was performed [20]. Briefly, a dorsal midline incision was made between the mid-back and tail base; the peritoneal cavity was accessed through bilateral muscle layer incisions; and the ovaries were identified, and the connection between the fallopian tube and the uterine horn was suture-ligated. After removal of the ovaries, wounds were closed.

Bilateral maxillary first molar (mxM1) extractions were performed. Briefly, molars were slowly elevated using micro-forceps, taking care to avoid root fractures. Bleeding was controlled by local compression. Teeth had to be extracted at ~ 6 weeks of age because the cementum accumulates at the root apices, making extraction progressively more difficult and traumatic in even slightly older animals. Consequently, 6-week-old mice were used for mxM1 extraction followed by OVX, then examined at multiple stages thereafter.

Osteotomies were performed in healed mxM1 sites using a 0.3-mm-diameter drill (Drill Bit City, USA) run at 1000 rpm, with saline irrigation.

Following surgeries, mice recovered in a heat-controlled environment. Mice were fed a soft food diet. No adverse post-operative events (e.g., abnormal swelling, severe pain, and infection) were observed.

Table 1 A comprehensive summary of experimental design (including Fig. 1, 2, 3, and 4 experiments). Experimental groups used in Fig. 1

Age (months)	Genotype	Vertebrae	Femur	Alveolar bone	Type of analysis	Minimum sample size* (*N*)	Actual sample size	Actual animal *N*	OVX	Age at time of surgery (months)
1.5	WT	x	x	x	μCT	4	8	4	No	NA
3.5	WT	x	x	x	μCT	4	8	4	No	NA
3.5	WT	x	x	x	μCT	4	8	4	Yes	1.5
> 12	WT	x	x	x	μCT	4	8	4	No	NA

* Minimum sample size required to sufficiently power the study; please see "Methods" and "Statistical analyses" for details

Imaging

Three-dimensional micro-computed tomographic (μCT) scanning followed guidelines [25]. Scanning was performed on vivaCT 40 data acquisition system (Scanco, Brüttisellen, Switzerland) at 10.5 μm voxel size (70 kV, 115 μA, and 300 ms integration time). Bone morphometry was performed using CTAn software (SkyScan, Belgium). 3D reconstructions were carried out using Avizo (FEI, Hillsboro, OR) and DataViewer (SkyScan, Belgium) software.

ELISA

Prior to the collection of blood, animals were fasted for 6 h. Each analysis required 100–200 μL of blood, collected from the infraorbital region. Blood was maintained at room temperature for 2 h, then centrifuged at 4000 rpm for 20 min. The supernatant containing sera was collected and stored at − 80 °C. The N-terminal propeptide of type I procollagen (PINP) served as a bone formation marker [26], and the C-terminal telopeptide of type I collagen (CTX-1) served as a bone resorption marker [26]. ELISA assays for PINP (Immunodiagnostic Systems, Tyne and Wear, UK, code AC-33F1) and CTX-1 (code AC-06F1) were carried out following the manufacturer's instructions.

Tissue collection, preparation, and sectioning

Immediately after euthanasia, tissues were washed in phosphate-buffered saline (PBS) then fixed into 4% paraformaldehyde (PFA). Mineralized tissues were decalcified in 10% EDTA solution in a microwave (Ted Pella Inc., CA, USA) at 25 °C for ~ 2 weeks. After decalcification, tissues were dehydrated by a graded ethanol series, embedded in paraffin, and sectioned using a Leica microtome (Leica Instruments GmbH, Hubloch, Germany).

Histology

Selected slides were deparaffinized (CitriSolv, #89426-268, VWR, Radnor, PA) then rehydrated. Pentachrome staining [14] was carried out, in which the mature osteoid matrix stains yellow, the new osteoid matrix stains green, the nuclei are black, and the muscle is red.

ALP and TRAP activities

Representative tissue sections were examined for tartrate-resistant acid phosphatase (TRAP) and alkaline phosphatase (ALP) activities. For ALP, tissues were treated with NBT/BCIP substrate (#34043, Thermo Scientific, USA). TRAP activity was detected by applying a solution from the TRAP staining kit (386A, Sigma, USA) and stored at 37 °C in a moist heated chamber. The duration of stainings was held constant for all samples.

Histomorphometric analyses

For all quantitative analyses, a region of interest (ROI) was established. In the lumbar vertebrae and in the interradicular

Table 2 A comprehensive summary of experimental design (including Fig. 1, 2, 3, and 4 experiments). Experimental groups used in Fig. 2a–f

Age	Genotype	M1 extraction	OVX	Age at time of M1 ext. and OVX	Healing period (months)	Sacrifice (months)	Type of analysis	Minimum sample size (*N*)	Actual sample size	Actual animal *N*	Experimental group
1.5	WT	Yes	No	1.5	1	2.5	μCT, histology	4	8	4	Young (Fig. 2b, c, f)
1.5	WT	Yes	Yes	1.5	2	3.5	μCT, histology	4	8	4	OVX (Fig. 2d–f)
1.5	WT	Yes	No	1.5	> 12	> 12	μCT	4	8	4	Aged (Fig. 2f)

Table 3 A comprehensive summary of experimental design (including Fig. 1, 2, 3, and 4 experiments). Experimental groups used in Fig. 2g–l

Age	Genotype	M1 ext	OVX	Age at time of M1 ext. and OVX	Osteotomy	Age at time of osteotomy (months)	Healing period (months)	Sacrifice (months)	Type of analysis	Minimum sample size (*N*)	Actual sample size	Actual animal *N*	Experimental group
1.5	WT	Yes	No	1.5	Yes	2.5	0.75	3.25	μCT, histology	4	8	4	Young (Fig. 2h–j)
1.5	WT	Yes	No	1.5	No	NA	NA	3.25	μCT		8		
1.5	WT	Yes	Yes	1.5	No	NA	NA	4.25	μCT	4	8	4	OVX (Fig. 2h, k, l)
1.5	WT	Yes	Yes	1.5	Yes	3.5	0.75	4.25	μCT, histology		8		

spaces around mxM1, the ROI was manually selected. For quantification of new bone formed in osteotomies, the ROI was manually selected along the edges of osteotomy sites.

Histomorphometric analyses were performed using Photoshop software (Ver. 19.0.0, Adobe, USA). All images were captured at ×40 magnification. Quantification and analyses were conducted by two blinded individuals. A minimum of six sections were analyzed for each staining. To quantify ALP-positive (ALP^{+ve}) or TRAP-positive ($TRAP^{+ve}$) cells, pixels corresponding to the staining were selected using the magic wand function. These values served as the numerator; the total number of pixels within the ROI served as the dominator. Values were therefore expressed as a percentage. Using ImageJ software (version 1.52k, NIH, USA) and tissue sections, the length of the trabecular surfaces was quantified and the number of either ALP- or TRAP-positive cells lining on the bone surface was manually identified. After quantification, the number of positive cells was normalized to the length of the trabecular surface.

To quantify the number of X-gal-positive ($X\text{-}gal^{+ve}$) cells, the same strategy was applied to selecting the $X\text{-}gal^{+ve}$ pixels; this value was divided by the total number of pixels in the ROI.

Staining with 4′,6-diamidino-2-phenylindole (DAPI) was used to identify viable cells in an osteotomy; DAPI-positive ($DAPI^{+ve}$) cells were then counted manually, and the resulting number served as the denominator. Cells immunopositive for Runx2 and for cathepsin K were counted manually; this number served as the numerator.

L-PBS and L-WNT3A

A split-mouth design was employed for these experiments, wherein liposomal PBS (L-PBS) was used to treat osteotomies on one side and liposomal WNT3A (L-WNT3A, 0.3 μg/ml) was used to treat the contralateral side of OVX mice. L-WNT3A was formulated as described [27] where human recombinant WNT3A protein was reconstituted in association with a liposome manufactured from DMPC and cholesterol. The activity of L-WNT3A was validated using an LSL assay wherein cells respond to a Wnt stimulus by expressing luciferase. Active L-WNT3A was then combined with a biphasic collagen gel (Life Technologies, NY, USA) that is in a liquid form at 4 °C and is in a gel form at 37 °C. Approximately 1 μl of collagen gel containing 0.3 ng of L-WNT3A was delivered to each osteotomy by Hamilton syringe injection. An

Table 4 A comprehensive summary of experimental design (including Fig. 1, 2, 3, and 4 experiments). Experimental groups used in Fig. 3

Age (months)	Genotype	OVX	Age at time of surgery (months)	Type of analysis	Minimum sample size (*N*)	Actual sample size	Actual animal *N**	Experimental group
3.5	WT	No	NA	ELISA, ALP, TRAP	3	4	4	Young group/control (Fig. 3a–c, f)
2.0	WT	Yes	1.5	ELISA	3	4	4	Week 2
2.5	WT	Yes	1.5	ELISA	3	4	4	Week 4
3.0	WT	Yes	1.5	ELISA	3	4	4	Week 6
3.5	WT	Yes	1.5	ELISA, ALP, TRAP	3	4	4	Week 8, OVX (Fig. 3a, b, d, g)
> 12	WT	No	NA	ELISA, ALP, TRAP	3	4	4	> 12 months old (Fig. 3a, b, e, h)

* Shared by animals utilized in the Fig. 1 experiment

equivalent volume of L-PBS was combined in the collagen gel and delivered to osteotomies; these served as the controls.

Immunohistochemistry

Slides were permeabilized with 0.5% Triton X-100. After antigen retrieval, blocking was carried out with 5% goat serum (S-1000, Vector) for 1 h at room temperature. Slides were incubated with primary antibodies at 4 °C overnight. Primary antibodies included anti-Osterix (ab22552, Abcam), anti-Runx2 (ab23981, Abcam), and anti-Cathepsin K (ab19027, Abcam). Following PBS washing, slides were incubated with Cyanine5-conjugated goat anti-rabbit secondary antibody (A10523, Invitrogen) for 1 h at room temperature, then mounted with a DAPI mounting medium (Vector Laboratories).

Statistical analyses

An online tool, designed for calculating the minimum sample size for adequate study power, was employed: https://clincalc.com/stats/SampleSize.aspx. The calculated minimum number of samples required for adequate study power is indicated in Tables 1, 2, 3, 4, and 5 under the heading "minimum sample size." The actual number of samples generated for each experiment is also shown in Tables 1, 2, 3, 4, and 5 under the heading "actual sample size." All estimations were performed by setting parameters so that α(type I error) = 0.05, β(type II error) = 0.2, and enrollment ratio = 1. Results are presented in the form of mean ± standard deviation, with N equal to the actual number of animals analyzed. All statistical analyses were performed using GraphPad 5.0 (GraphPad Software, San Diego, CA). Histomorphometric analyses utilized Student's t test (comparisons between the 3.5-month-old young control group and the > 12-month-old group in Figs. 3a and Fig. 4F, Q) and one-way ANOVA (all other comparisons). Tukey's test was performed as the post hoc test. Significance was attained at $p < 0.05$. In addition, a post hoc power analysis tool (https://clincalc.com/stats/Power.aspx) was then employed to verify the power of our results. All comparisons are powered > 95%.

Results

OVX mice exhibit an accelerated aging phenotype in all skeletal tissues

An experimentally induced model mimicking bone loss in osteoporosis has been established [20] whereby removal of the ovaries in young rodents leads to a dramatic decrease in bone mass and bone mineral density. We began monitoring bony changes in mice, beginning during the growth phase

Table 5 A comprehensive summary of experimental design (including Fig. 1, 2, 3, and 4 experiments). Experimental groups used in Fig. 4

Age (M)	Genotype	M1 ext	Age at time of M1 ext. (M)	OVX	Age at time of OVX (M)	Osteotomy	Age at time of osteotomy (M)	Treatment	Sacrifice (M)	Type of analysis	Minimum sample size (N)	Actual sample size	Actual animal N	Exp. group
1.5	WT	Yes	1.5	No	NA	Yes	3.5	None	3.75	Histology	3	6	3	Young (Fig. 4B)
1.5	WT	Yes	1.5	Yes	1.5	Yes	3.5	None	3.75	Histology		6	3	OVX (Fig. 4D)
1.5	Axin2$^{LacZ/+}$	Yes	1.5	No	NA	Yes	3.5	None	3.75	Xgal	3	6	3	Young (Fig. 4C, F)
1.5	Axin2$^{LacZ/+}$	Yes	1.5	Yes	1.5	Yes	3.5	None	3.75	Xgal		6	3	OVX (Fig. 4E, F)
1.5	WT	Yes	1.5	Yes	1.5	Yes	3.5	L-PBS	3.75	µCT histology IHC	4	6	6	L-PBS, day 7 (Fig. 4G, G′ I, K, M, O, Q, R, R′)
1.5	WT	Yes	1.5	Yes	1.5	Yes	3.5	L-WNT3A	3.75	µCT histology IHC		6		L-WNT3A, day 7 (Fig.4H, H′,J, L, N, P, Q, R, R′)
1.5	WT	Yes	1.5	Yes	1.5	Yes	3.5	L-PBS	4	µCT	4	6	6	L-PBS, day 14 (Fig. 4R, R′)
1.5	WT	Yes	1.5	Yes	1.5	Yes	3.5	L-WNT3A	4	µCT		6		L-WNT3A, day 14 (Fig. 4R, R′)
1.5	WT	Yes	1.5	Yes	1.5	Yes	3.5	L-PBS	4.25	µCT, histology	4	6	6	L-PBS, day 21 (Fig. 4R, R′, S, S′)
1.5	WT	Yes	1.5	Yes	1.5	Yes	3.5	L-WNT3A	4.25	µCT, histology		6		L-WNT3A, day 21 (Fig. 4R, R′, T, T′, V)

prior to skeletal maturation [28]. Between 1.5 (Fig. 1a, b) and 3.5 months of age (Fig. 1c, d), bone mass increases in the lumbar vertebrae and in the distal femur. When the ovariectomy (OVX) procedure was performed in 1.5-month-old mice, growth-related bone accrual was hindered (compare Fig. 1c, d with Fig. 1e, f). From a structural perspective, the bone loss observed in OVX mice was an accelerated version of the bone loss that occurred with natural aging (Fig. 1g, h).

OVX also induced alveolar bone loss. Normally between 1.5 months (Fig. 1i) and 3.5 months (Fig. 1j) of age, there is a modest increase in BV/TV from 80.8% ± 5.5% to 81.2% ± 4.1% in the jawbones (Fig. 1m); this change, however, is not statistically significant. When 1.5-month-old mice underwent OVX, there was a dramatic, significant loss in alveolar bone density (Fig. 1k). From a structural perspective, this OVX-induced bone loss mirrored the alveolar bone loss that occurred in aged mice (Fig. 1l).

Quantification of alveolar BV/TV captured these changes in bone density (Fig. 1m). Comparing the OVX group with the aged group, we noted that the percent decrease in BV/TV was equivalent (Fig. 1m). Relative to young mice, trabecular thickness was significantly decreased in the OVX and aged groups (Fig. 1n). Trabecular number did not change significantly among the groups (Fig. 1o), but trabecular separation was significantly increased in the OVX and aged groups, relative to the young group (Fig. 1p). Thus, OVX mice exhibited structural changes in alveolar bone architecture which were similar to age-related changes in mice.

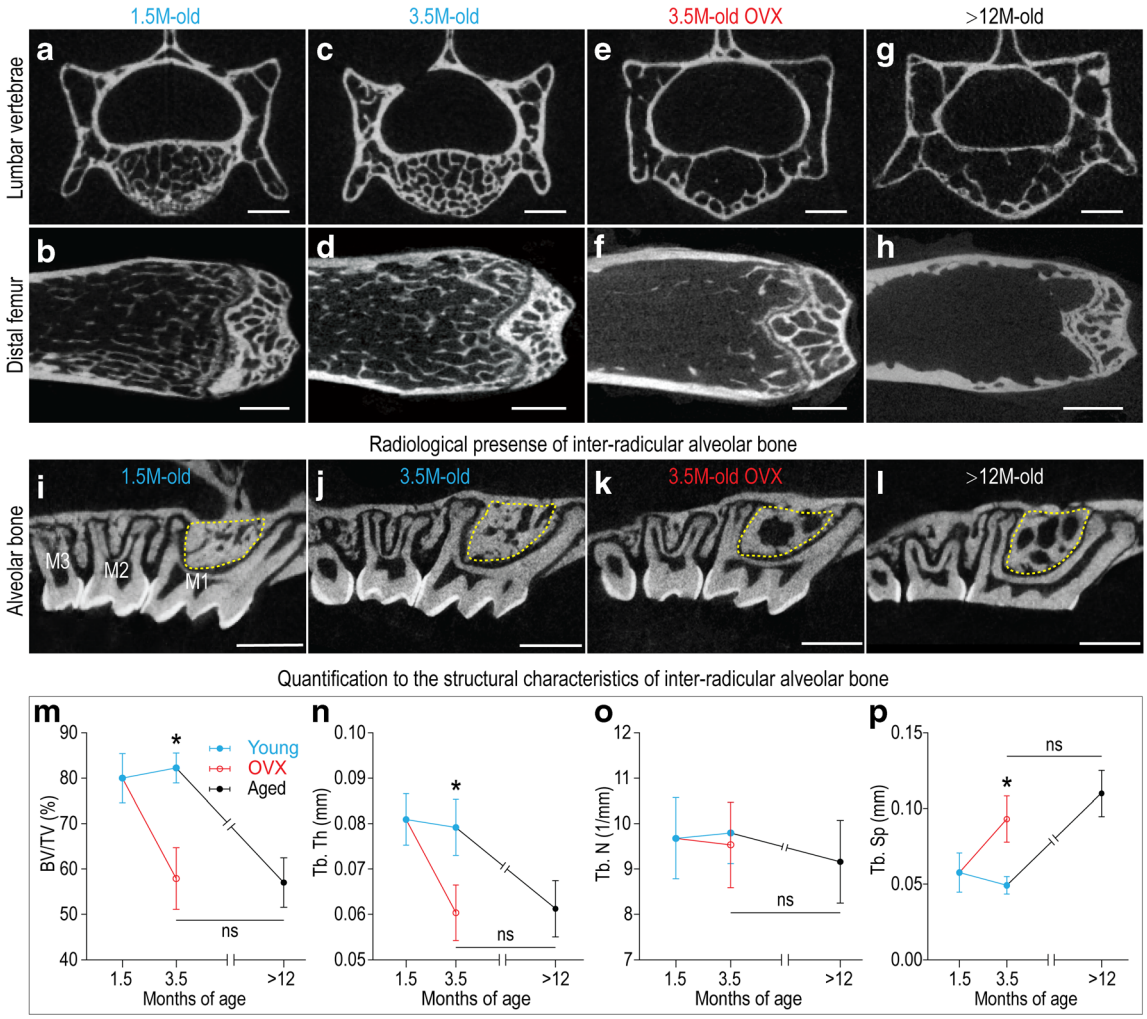

Fig. 1 OVX mice exhibit an accelerated aging skeleton phenotype. Representative μCT sections showing the **a** lumbar vertebrae and **b** distal femur in a 1.5-month-old mouse, **c**, **d** in a 3.5-month-old mouse, **e**, **f** in a 3.5-month-old OVX mouse, and **g**, **h** in a > 12-month-old mouse. Representative sagittal μCT sections showing the interradicular alveolar bone around the maxillary first molar (mxM1) in a 1.5-month-old mouse (**i**), a 3.5-month-old mouse (**j**), a 3.5-month-old OVX mouse (**k**), and a > 12-month-old mouse (**l**). Focusing on the interradicular space around the mxM1, we measured the following parameters at all time points: **m** BV/TV, **n** Tb.Th, **o** Tb.N., and **p** Tb.Sp. within the region indicated with the dotted yellow line. Abbreviations: 1.5/3.5/>12M-old, 1.5/3.5/>12-month-old; OVX, ovariectomy; M1/2/3, maxillary first/second/third molar; BV/TV, bone volume/total volume; Tb.Th, trabecular thickness; Tb.N, trabecular number; Tb.Sp, trabecular separation; ns: no statistical difference. Scale bars = 1 mm. Asterisks: statistical difference of the 3.5-month-old young group versus 3.5-month-old OVX group

Alveolar bone with an osteoporotic-like phenotype is associated with delayed extraction socket healing

One means by which to assess whether experimentally induced osteoporotic-like changes affected alveolar bone repair was to evaluate the rate of extraction socket healing. While the anatomy of the healing site is complex, the shape and size of teeth do not change significantly with age. Consequently, the rate of bony fill could be directly compared between animals of different ages. Therefore, bilateral mxM1 tooth extractions were performed; in the young control group, mice were 1.5 months old at the time of tooth extraction (blue triangle, Fig. 2a). In the OVX group, mice were also 1.5 months old when they underwent tooth extraction and OVX surgery (blue and red triangles, Fig. 2a). Healing was assessed by μCT and histology at post-operative weeks 4 and 8 (Fig. 2a). In the young control group, extraction sites were healed by week 4 (Fig. 2b, c). In the OVX group, extraction sites took 8 weeks to heal (Fig. 2d, e).

Extraction socket repair was delayed in OVX mice, but did they eventually heal? The answer was yes; by comparing the BV/TV of pristine interradicular bone (lighter colored bars, Fig. 2f) with BV/TV of healed sites, it was clear that young, OVX, and aged mice all exhibited complete repair of their extraction sockets, e.g., the BV/TV of healed sites matched that of intact interradicular bone nearby (darker-colored bars, Fig. 2f).

We verified that the OVX-related delay in alveolar bone repair was not unique to an extraction socket model by performing another common dental procedure, e.g., producing an osteotomy. Once again, young control mice were 1.5 months old at the time of tooth extraction (blue triangle, Fig. 2g). In the OVX group, mice were also 1.5 months old when they underwent tooth extraction and OVX surgery (blue and red triangles, Fig. 2g). To establish an equivalent baseline for both groups, we allowed the OVX group to reach complete healing. Thereafter, osteotomies were produced in young and OVX groups using the same-sized drill, run at the same rotational velocity with irrigation (yellow triangle, Fig. 2g). Three weeks later, osteotomies were assessed for evidence of bone healing (black triangles, Fig. 2g). In the young control group, osteotomy healing was complete by week 3 (blue bars, Fig. 2i–j). Osteotomies produced in the OVX group had not completed healing by week 3 (red bars, Fig. 2h; see also Fig. 2k, l). Therefore, we concluded that regardless of the type of injury, OVX was associated with slower alveolar bone repair.

OVX alters bone resorptive activity without a significant depression in bone formation

We wanted to gain insights into why bone repair was slower in the OVX group compared to the young control group. We began by exploring when the first changes in new bone formation rates were detectable using the anabolic marker N-terminal propeptide of type I procollagen (PINP), and the catabolic marker, C-terminal telopeptide of type I collagen (CTX-1). We confirmed that PINP and CTX-1 were reliable indicators of changes in bone formation and bone resorption activities, by comparing their serum levels in the young control group, the OVX group, and the aged group. As expected, relative to 3.5-month-old young mice, those that were > 12 months old had reduced PINP levels (light blue bar, Fig. 3a) and elevated CTX-1 levels (light pink bar, Fig. 3a).

The OVX group was examined next. Two weeks after OVX, CTX-1 levels were nearly 3 times that normally observed in young, 3.5-month-old control mice (Fig. 3a). PINP levels were also elevated relative to the control mice (Fig. 3a). Throughout the period of evaluation, CTX-1 serum levels remained significantly higher in the OVX compared to young controls (Fig. 3a), indicating persistent bone resorption in the OVX cohort. PINP levels, on the other hand, gradually returned to levels observed in the young control group (Fig. 3a).

Alkaline phosphatase (ALP) and tartrate-resistant acid phosphatase (TRAP) activities were monitored using histomorphometric analyses, and the resulting data are presented in two ways: first, we manually identified ALP^{+ve} or $TRAP^{+ve}$ pixels and divided these numbers by the total number of pixels in a given ROI (Fig. 3b). Second, the ALP^{+ve} or $TRAP^{+ve}$ cell numbers were divided by the lengths of the trabecular surfaces on which they were attached; this showed the relative distribution of bone-resorbing and bone-forming cells in the young, OVX, and aged groups (Fig. 3b). Both datasets mirrored ELISA results: namely, ALP activity was high in the young control group (Fig. 3c), high in the OVX group (Fig. 3d), and low in the aged group (Fig. 3e). conversely, TRAP activity was lowest in the young group (Fig. 3f) and significantly higher in the OVX and aged groups (Fig. 3g, h). Collectively, these results demonstrated that OVX produced a skeletal phenotype that aligned with an osteoporotic phenotype, primarily by amplifying bone resorption. In this way, OVX-induced condition mimicked age-related bone loss. On the other hand, OVX did not have a significant impact on bone formation rates, and in this regard the OVX-induced bony phenotype stood in sharp contrast to age-related osteoporosis.

L-WNT3A accelerates bone repair in a model with osteoporotic-like phenotype

Like age-related bone loss, the phenotype induced by OVX is characterized by persistent, elevated bone resorption; unlike the age-related disease, OVX-induced bone loss has a normal level of new bone formation. Why then is healing slower in OVX mice? If bone formation rates were unchanged in OVX mice, then the initial stages of repair should have been equivalent to the young control group. We hypothesized that OVX

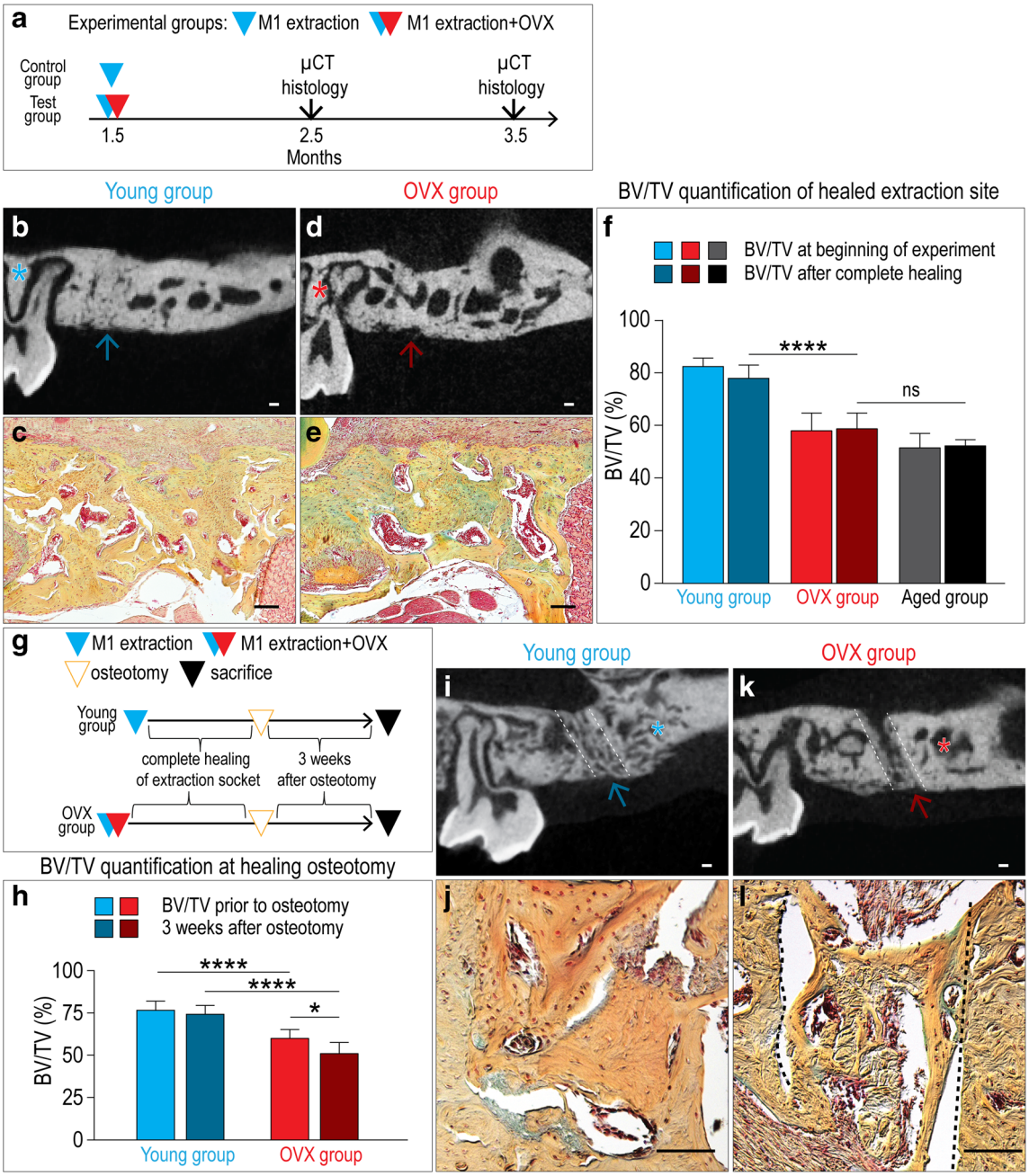

Fig. 2 An OVX-related osteoporotic-like phenotype is associated with delayed alveolar bone repair. **a** Schematic illustration of maxillary first molar (mxM1) extraction. **b** Representative sagittal μCT and **c** pentachrome-stained sections showing a healed extraction socket in the young group and OVX group (**d**, **e**). **f** BV/TV quantitation of the healed extraction site in young, OVX, and aged groups. **g** Schematic illustration of the osteotomy experiment. **h** BV/TV comparison between pristine interradicular bone and healed osteotomy site on post-osteotomy week 3 in both young and OVX groups. **i** Representative sagittal μCT and **j** pentachrome-stained sections on post-osteotomy week 3 in the young group and OVX group (**k**, **l**). Arrows (for healed mxM1 extraction site or osteotomy) and asterisks (for pristine bone) indicate the ROIs. Abbreviation: M1, maxillary first molar; OVX, ovariectomy; BV/TV, bone volume/total volume; ns, no statistical difference. Scale bars = 100 μm. *$p < 0.05$; ****$p < 0.0001$

caused a decline in endogenous Wnt signaling, and the reasoning behind this hypothesis was as follows: endogenous Wnt signaling is required to maintain bone mass [29], and a direct consequence of amplified Wnt signaling is bone accrual [30]. Conversely, reduced Wnt signaling is associated with low bone mass conditions including osteoporosis [31, 32]. We conjectured that a decline in endogenous Wnt signaling might also be a hallmark of the bone mass decline in the OVX model, and therefore, we used a strain of Wnt reporter mice, and an osteotomy injury model, to test whether this was true. Young and OVX groups of mice underwent mxM1 extraction; when the extraction sites were completely healed, osteotomies

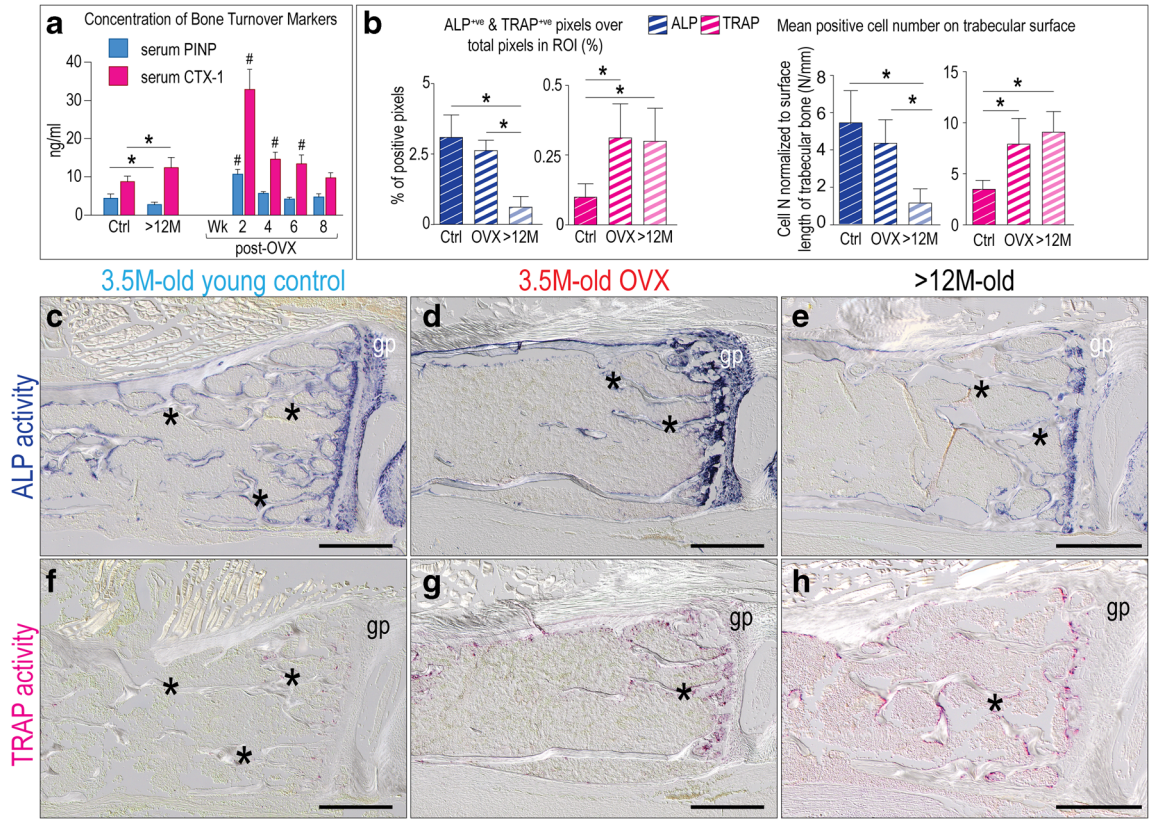

Fig. 3 OVX induces bone resorption without significantly depressing bone formation. **a** Quantification of the bone formation marker N-terminal propeptide of type I procollagen (PINP) and C-terminal telopeptide of type I collagen (CTX-1) in sera harvested from the 3.5-month-old young control group, > 12-month-old group, and 3.5-month-old OVX mice at multiple post-OVX time points. **b** Quantification of the percentage of ALP^{+ve} and $TRAP^{+ve}$ pixels over total pixels in the region of interest (ROI). Data are also presented as ALP^{+ve} and TRAP $^{+ve}$ cell numbers normalized to the surface length of trabecular bone in the lumbar vertebrae. Representative sagittal sections showing the lumbar vertebrae in a 3.5-month-old young control (**c**), 3.5-month-old OVX (**d**), and > 12-month-old group (**e**) stained to detect ALP activity. **f**–**h** Adjacent sections stained with TRAP. Asterisks identify trabeculae in panels **c**–**h**. Abbreviation: Ctrl, 3.5 month-old young control; >12M, > 12-month-old; post-OVX, post ovariectomy; wk, week; gp, vertebral growth plate. Scale bars = 500 μm. * in panels **a** and **b** indicates $p < 0.05$; # in panel **a** indicates statistical difference versus 3.5-month-old young control, $p < 0.05$

were produced; 1 week later, the partially healed sites were evaluated for the presence of Wnt-responsive cells (Fig. 4A). When the injuries were produced in *Axin2*$^{LacZ/+}$ mice, the Wnt-responsive cells could be identified by virtue of β-galactosidase expression, which when subjected to X-gal staining renders them blue. In the young control group, the osteotomy healed partially (Fig. 4B) and X-gal^{+ve} Wnt-responsive osteoblasts were populated in the osteotomy (Fig. 4C). In the OVX group, there was scant evidence of new bone (Fig. 4D), and few X-gal^{+ve} cells were detectable (Fig. 4E; quantified in Fig. 4F).

We tested if delivery of a Wnt protein therapeutic was sufficient to return healing rates in an OVX animal back to those observed in young rodents. Osteotomies were produced in OVX rodents then treated with either a liposomal formulation of WNT3A protein (L-WNT3A) or an identical liposome formulation containing PBS (L-PBS; Fig. 4A).

As early as post-osteotomy day 7, the new osteoid matrix was evident in L-WNT3A-treated sites (compare Fig. 4G, G′, H, H′). Histologic assessment verified μCT data: L-PBS-treated osteotomies were filled with fibroblasts (Fig. 4I) while L-WNT3A-treated sites were occupied with bone (Fig. 4J). Osteoclast activity, as shown by cathepsin K expression [33], was repressed by L-WNT3A treatment (compare Fig. 4K, L) while osteogenic gene expression, as shown by Runx2 (Fig. 4M, N) and Osterix (Fig. 4O, P) expression, was enhanced by L-WNT3A treatment (Fig. 4Q).

Both BV/TV and bone mineral density (BMD) were increased in response to L-WNT3A treatment (Fig. 4R, R′). By post-osteotomy day 21, L-PBS-treated sites in OVX mice were still not completely healed (Fig. 4S, S′), whereas the L-WNT3A-treated sites in OVX mice were (Fig. 4T, T′). Histologically, the appearance of L-WNT3A-treated osteotomies was on par with healed osteotomies in the young cohort (compare Fig. 4U, V). Thus, we conclude that L-WNT3A treatment accelerated bone healing in an OVX model of alveolar bone repair, back to levels observed in young animals.

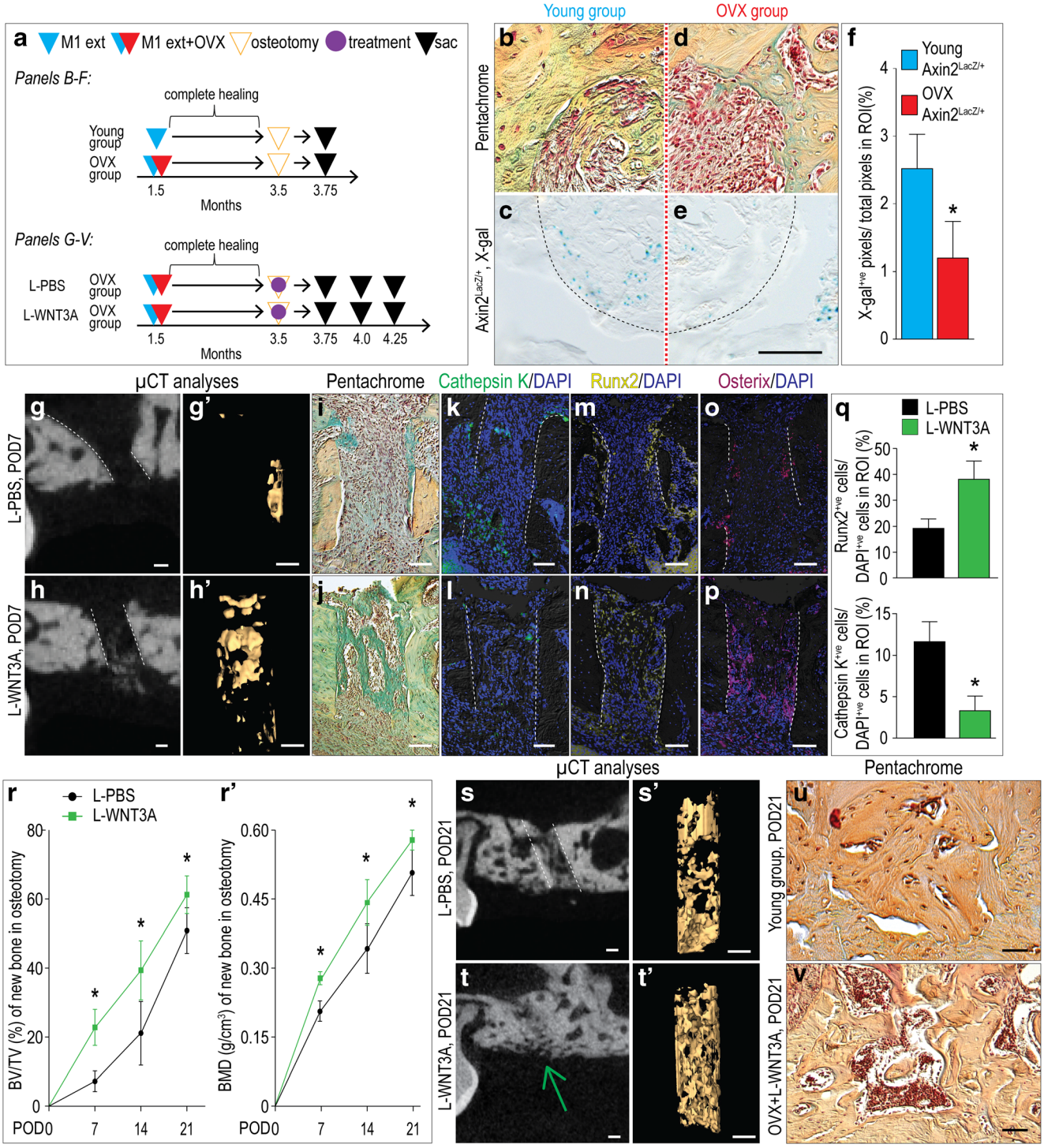

Discussion

Distinctions between OVX-induced and age-related bone loss

We show here, as others have before us [7, 34], that OVX induces a severe bone loss in the axial, appendicular, and craniomaxillofacial skeletons of mice (Fig. 1). The deterioration we observe in the skeletons of young mice in response to OVX shares many similarities with the age-related skeletal deterioration (Fig. 1), leading many clinicians and scientists to conclude that rodents, like humans, can exhibit osteoporosis [34–36]. Nonetheless, we refer to this as an "osteoporotic-like condition" because despite best efforts [37, 38], there is still no universal definition for a diagnosis of osteoporosis in animals.

◀ **Fig. 4** Accelerated bone formation via L-WNT3A in an OVX-related bone loss model. (a) Schematic of the experimental design. On post osteotomy day (POD) 7, representative transverse tissue sections (b) from a young wild-type mouse stained with pentachrome to show a new bone matrix and (c) from a young $Axin2^{LacZ/+}$ mouse stained with X-gal to reveal the distribution of Wnt-responsive cells in the osteotomy. On POD7, representative transverse tissue sections (d) from an OVX wild-type mice to show a cellular infiltrate in the osteotomy and (e) from an OVX $Axin2^{LacZ/+}$ mice stained with X-gal. (f) Quantification of X-gal-positive ($X\text{-}gal^{+ve}$) pixels within osteotomies from young $Axin2^{LacZ/+}$ and OVX $Axin2^{LacZ/+}$ mice. (g) Representative μCT sections and (g′) 3D reconstruction of osteotomies on POD7, following treatment with L-PBS or (h, h′) L-WNT3A. (i, j) Representative tissue sections from both treated osteotomies, stained with pentachrome, and immunostained with (k, l) cathepsin K, (m, n) Runx2, and (o, p) osterix. In all panels, DAPI staining was quantified as a means to determine the number of viable cells in the ROI of the osteotomy. (q) Quantification of both Runx2 and cathepsin K–positive cells in the ROIs. (r, r′) BV/TV and BMD in the osteotomies as a function of time and treatment. (s) On POD21, representative μCT sections and (s′) 3D reconstruction of osteotomies following treatment or L-PBS (t, t′) L-WNT3A. Representative sagittal tissue sections from (u) a young mouse and (v) an OVX mouse treated with L-WNT3A, stained with pentachrome to show complete healing of the osteotomy on POD21. Abbreviations: OVX, ovariectomy; ext, extraction; BV/TV, bone volume/total volume; BMD, bone mineral density. Green arrow indicates the complete healed osteotomy site. Scale bar, 100 μm; $*p < 0.05$

We provide data demonstrating that aged-related bone loss and OVX-induced bone loss are not identical conditions. We showed that the age-related condition in mice is characterized by a reduction in bone-forming capacity, simultaneous with a gain in bone-resorbing activity (Fig. 3), analogous to what has been reported in osteoporotic patient populations [39, 40]. Bone-resorbing activity is also increased in OVX-induced bone loss (Fig. 3), but unlike age-related bone loss, we showed that there was no concomitant decrease in bone-forming activity (Fig. 3). This latter finding may have implications for the testing of anabolic therapies designed to stimulate new bone formation in osteoporotic patients, and along these lines, we considered the validity of rodent OVX models as surrogates for human osteoporosis. Another caveat to these data was the fact that animals used in this study were necessarily quite young, e.g., 6 weeks of age rather than 8 weeks of age [7, 41, 42]. This young age was necessary because tooth extraction in older rodents is complicated by cementum accumulation. When attempting to extract teeth in even slightly older rodents, the result is oftentimes fracturing of the alveolar bone and retention of tooth root fragments, both of which complicate healing and are unnecessarily injurious to the animal.

Performing an OVX on 6-week-old mice had a modest, but not significant effect on growth-related bone accrual (Fig. 1). Others have performed OVX on young animals and demonstrated a delay in fracture healing [7]. If the investigators then compared the rate of delayed healing in the young OVX cohort against healing in older cohorts of OVX animals, the older groups healed even slower [7]. When considering the potential clinical relevance of data shown here, and comparing it against the published literature, our data likely under-reports the impact of OVX on alveolar bone healing rates.

Alveolar bone with osteoporotic-like phenotype can heal completely, just at a slower rate

There remains a considerable knowledge gap about the impact of osteoporosis/osteopenia on alveolar bone health, and this uncertainty presents a challenge for dental professionals whose patient populations are > 50 years of age [18]. While some clinical studies conclude that patients with osteoporosis show no delay in healing or in implant osseointegration [43], other studies clearly caution readers about age-related alveolar bone loss [44]. Our study in OVX mice demonstrated that extraction sockets and osteotomies healed significantly slower than young controls (Fig. 2). Does this difference represent a species-specific disparity between mice and humans? Alternatively, it could represent a difference between OVX-induced osteoporotic-like conditions, shown here in rodents, and the age-related osteoporosis exhibited in patient populations.

L-WNT3A as a therapeutic to promote alveolar bone healing

In animals with severe bone loss, including humans, bone resorption predominates over bone formation, leading to a gradual but inevitable decline in bone density. Why is a single, local exposure to L-WNT3A sufficient to accelerate new bone formation in an osteotomy? The answer, we believe, lies in an examination of the early phases of healing (Fig. 4). Compared to L-PBS-treated osteotomies in OVX mice, L-WNT3A-treated osteotomies have considerably more osteoprogenitor cells, and considerably fewer osteoclasts, than osteotomies treated with L-PBS (Fig. 4). By expanding this population of proliferating osteoprogenitor cells, L-WNT3A tipped the balance in favor of faster bone repair (Fig. 4).

It is equally important to note that at later stages, differences between the L-WNT3A- and L-PBS-treated groups narrowed (Fig. 4). There are two likely explanations: first, a single dose of L-WNT3A is delivered immediately after osteotomy so the beneficial effects are most certainly transient. Second, bone loss in OVX mice is primarily related to elevated bone resorption and it is likely that this systemic effect dominates over longer time frames. Fortunately, it appears that once an implant achieves osseointegrated, maintenance of that status is not unduly impacted by osteoporosis.

There is a third possibility, which we favor. In patient populations, the intervals at which healing is assessed are often quite long, on the order of 5 years or more. This interval

precludes any determination of whether there is an actual delay in bone repair or osseointegration [45].

Conclusion

With the limitations of this study, our data show that despite a severe bone loss phenotype, mice completely healed both extraction sockets and alveolar bone osteotomies, provided sufficient time between the injury and the examination of healing is allowed to elapse (Fig. 2). Treating the osteotomies with a liposomal formulation of WNT3A significantly accelerated new alveolar bone formation in OVX mice. These preclinical data, we believe, may have clinical implications: in systemic bone loss conditions such as osteoporosis, dental professionals should factor into their treatment planning sufficient time to allow complete healing prior to reconstructive procedures such as dental implant therapy.

Acknowledgments We thank Bo Liu, Xue Yuan, Xiaohui Zhang, and Quanchen Xu for their invaluable help with histology and data analysis.

Funding information This research project was supported by a grant from the National Institutes of Health (R01DE024000-11, J.A.H.), a grant from the National Key Research and Development Program of China (2016YFC1102702; L.W. and C.B.), and a grant from the National Natural Science Foundation of China (81600910; L.W.). Salary support for Y.L. was provided by L.W. and C.B. Funding to support this research was provided by J.A.H.

Compliance with ethical standards

The Stanford Committee on Animal Research approved all procedures, which conform to ARRIVE guidelines.

Conflicts of interest None.

References

1. Unnanuntana A, Gladnick BP, Donnelly E, Lane JM (2010) The assessment of fracture risk. J Bone Joint Surg Am 92:743–753
2. Zimmermann EA, Busse B, Ritchie RO (2015) The fracture mechanics of human bone: influence of disease and treatment. Bonekey Rep 4:743
3. Osterhoff G, Morgan EF, Shefelbine SJ, Karim L, McNamara LM, Augat P (2016) Bone mechanical properties and changes with osteoporosis. Injury 47(Suppl 2):S11–S20
4. Currey JD, Brear K, Zioupos P (1996) The effects of ageing and changes in mineral content in degrading the toughness of human femora. J Biomech 29:257–260
5. Giannoudis P, Tzioupis C, Almalki T, Buckley R (2007) Fracture healing in osteoporotic fractures: is it really different? A basic science perspective. Injury 38(Suppl 1):S90–S99
6. Lill CA, Hesseln J, Schlegel U, Eckhardt C, Goldhahn J, Schneider E (2003) Biomechanical evaluation of healing in a non-critical defect in a large animal model of osteoporosis. J Orthop Res 21:836–842
7. Meyer RA Jr, Tsahakis PJ, Martin DF, Banks DM, Harrow ME, Kiebzak GM (2001) Age and ovariectomy impair both the normalization of mechanical properties and the accretion of mineral by the fracture callus in rats. J Orthop Res 19:428–435
8. Nikolaou VS, Efstathopoulos N, Kontakis G, Kanakaris NK, Giannoudis PV (2009) The influence of osteoporosis in femoral fracture healing time. Injury 40:663–668
9. Recovering from a broken bone. Royal Osteoporosis Society (2019) https://theros.org.uk/information-and-support/living-with-osteoporosis/recovering-from-a-broken-bone/. Accessed May 6 2019
10. Clark D, Nakamura M, Miclau T, Marcucio R (2017) Effects of aging on fracture healing. Curr Osteoporos Rep 15:601–608
11. Franceschi C, Garagnani P, Parini P, Giuliani C, Santoro A (2018) Inflammaging: a new immune-metabolic viewpoint for age-related diseases. Nat Rev Endocrinol 14:576–590
12. Schultz MB, Sinclair DA (2016) When stem cells grow old: phenotypes and mechanisms of stem cell aging. Development 143:3–14
13. Ganguly P, El-Jawhari JJ, Giannoudis PV, Burska AN, Ponchel F, Jones EA (2017) Age-related changes in bone marrow mesenchymal stromal cells: a potential impact on osteoporosis and osteoarthritis development. Cell Transplant 26:1520–1529
14. Chen CH, Wang L, Serdar Tulu U et al (2018) An osteopenic/osteoporotic phenotype delays alveolar bone repair. Bone 112:212–219
15. Arioka M, Zhang X, Li Z, Tulu US, Liu Y, Wang L, Yuan X, Helms JA (2019) Osteoporotic changes in the periodontium impair alveolar bone healing. J Dent Res 98:450–458
16. Mavropoulos A, Rizzoli R, Ammann P (2007) Different responsiveness of alveolar and tibial bone to bone loss stimuli. J Bone Miner Res 22:403–410
17. Giro G, Chambrone L, Goldstein A, Rodrigues JA, Zenobio E, Feres M, Figueiredo LC, Cassoni A, Shibli JA (2015) Impact of osteoporosis in dental implants: a systematic review. World J Orthop 6:311–315
18. Austin S, Bailey D, Chandu A, Dastaran M, Judge R (2015) Analysis of commonly reported medical conditions amongst patients receiving dental implant therapy in private practice. Aust Dent J 60:343–352
19. Sozen T, Ozisik L, Basaran NC (2017) An overview and management of osteoporosis. Eur J Rheumatol 4:46–56
20. Kalu DN, Chen C (1999) Ovariectomized murine model of postmenopausal calcium malabsorption. J Bone Miner Res 14:593–601
21. Liu B, Hunter DJ, Rooker S, Chan A, Paulus YM, Leucht P, Nusse Y, Nomoto H, Helms JA (2013) Wnt signaling promotes Muller cell proliferation and survival after injury. Invest Ophthalmol Vis Sci 54:444–453
22. Jho EH, Zhang T, Domon C, Joo CK, Freund JN, Costantini F (2002) Wnt/beta-catenin/Tcf signaling induces the transcription of Axin2, a negative regulator of the signaling pathway. Mol Cell Biol 22:1172–1183
23. Workman P, Aboagye EO, Balkwill F et al (2010) Guidelines for the welfare and use of animals in cancer research. Br J Cancer 102:1555–1577
24. Dutta S, Sengupta P (2016) Men and mice: relating their ages. Life Sci 152:244–248
25. Bouxsein ML, Boyd SK, Christiansen BA, Guldberg RE, Jepsen KJ, Muller R (2010) Guidelines for assessment of bone microstructure in rodents using micro-computed tomography. J Bone Miner Res 25:1468–1486
26. Naylor K, Eastell R (2012) Bone turnover markers: use in osteoporosis. Nat Rev Rheumatol 8:379–389
27. Dhamdhere GR, Fang MY, Jiang J et al (2014) Drugging a stem cell compartment using Wnt3a protein as a therapeutic. PLoS One 9:e83650

28. Jilka RL (2013) The relevance of mouse models for investigating age-related bone loss in humans. J Gerontol A Biol Sci Med Sci 68: 1209–1217
29. Baron R, Kneissel M (2013) WNT signaling in bone homeostasis and disease: from human mutations to treatments. Nat Med 19:179–192
30. Gong Y, Slee RB, Fukai N et al (2001) LDL receptor-related protein 5 (LRP5) affects bone accrual and eye development. Cell 107:513–523
31. Canalis E (2013) Wnt signalling in osteoporosis: mechanisms and novel therapeutic approaches. Nat Rev Endocrinol 9:575–583
32. Karasik D, Rivadeneira F, Johnson ML (2016) The genetics of bone mass and susceptibility to bone diseases. Nat Rev Rheumatol 12: 323–334
33. Wilson SR, Peters C, Saftig P, Bromme D (2009) Cathepsin K activity-dependent regulation of osteoclast actin ring formation and bone resorption. J Biol Chem 284:2584–2592
34. Thompson DD, Simmons HA, Pirie CM, Ke HZ (1995) FDA guidelines and animal models for osteoporosis. Bone 17:125S–133S
35. Komori T (2015) Animal models for osteoporosis. Eur J Pharmacol 759:287–294
36. Turner RT, Maran A, Lotinun S, Hefferan T, Evans GL, Zhang M, Sibonga JD (2001) Animal models for osteoporosis. Rev Endocr Metab Disord 2:117–127
37. Heiss C, Govindarajan P, Schlewitz G et al (2012) Induction of osteoporosis with its influence on osteoporotic determinants and their interrelationships in rats by DEXA. Med Sci Monit 18: BR199–BR207
38. Srivastava M, Mandal SK, Sengupta S, Arshad M, Singh MM (2008) Quantification of bone mineral density to define osteoporosis in rat. J Endocrinol Investig 31:393–399
39. Sowers MR, Zheng H, Greendale GA, Neer RM, Cauley JA, Ellis J, Johnson S, Finkelstein JS (2013) Changes in bone resorption across the menopause transition: effects of reproductive hormones, body size, and ethnicity. J Clin Endocrinol Metab 98:2854–2863
40. Demontiero O, Vidal C, Duque G (2012) Aging and bone loss: new insights for the clinician. Ther Adv Musculoskelet Dis 4:61–76
41. Zhou S, Wang G, Qiao L et al (2018) Age-dependent variations of cancellous bone in response to ovariectomy in C57BL/6J mice. Exp Ther Med 15:3623–3632
42. Song L, Bi YN, Zhang PY, Yuan XM, Liu Y, Zhang Y, Huang JY, Zhou K (2017) Optimization of the time window of interest in ovariectomized imprinting control region mice for antiosteoporosis research. Biomed Res Int 2017:8417814, p 10. https://doi.org/10.1155/2017/8417814
43. Sendyk DI, Rovai ES, Pannuti CM, Deboni MC, Sendyk WR, Wennerberg A (2017) Dental implant loss in older versus younger patients: a systematic review and meta-analysis of prospective studies. J Oral Rehabil 44:229–236
44. de Medeiros F, Kudo GAH, Leme BG, Saraiva PP, Verri FR, Honorio HM, Pellizzer EP, Santiago Junior JF (2018) Dental implants in patients with osteoporosis: a systematic review with meta-analysis. Int J Oral Maxillofac Surg 47:480–491
45. Compton SM, Clark D, Chan S, Kuc I, Wubie BA, Levin L (2017) Dental implants in the elderly population: a long-term follow-up. Int J Oral Maxillofac Implants 32:164–170